JACS
JOURNAL OF THE AMERICAN CHEMICAL SOCIETY
Article
pubs.acs.org/JACS

Reaction of *cis*-3-Chloroacrylic Acid Dehalogenase with an Allene Substrate, 2,3-Butadienoate: Hydration via an Enamine

Gottfried K. Schroeder,[‡] William H. Johnson, Jr.,[‡] Jamison P. Huddleston,[‡] Hector Serrano,[‡] Kenneth A. Johnson,[§,∥] and Christian P. Whitman*[,‡,∥]

[‡]Division of Medicinal Chemistry, College of Pharmacy, and [§]Department of Chemistry and Biochemistry, [∥]Institute for Cellular and Molecular Biology, University of Texas, Austin, Texas 78712, United States

Supporting Information

ABSTRACT: *cis*-3-Chloroacrylic acid dehalogenase (*cis*-CaaD) catalyzes the hydrolytic dehalogenation of *cis*-3-haloacrylates to yield malonate semialdehyde. The enzyme processes other substrates including an allene (2,3-butadienoate) to produce acetoacetate. In the course of a stereochemical analysis of the *cis*-CaaD-catalyzed reaction using this allene, the enzyme was unexpectedly inactivated in the presence of $NaBH_4$ by the reduction of a covalent enzyme–substrate bond. Covalent modification was surprising because the accumulated evidence for *cis*-CaaD dehalogenation favored a mechanism involving direct substrate hydration mediated by Pro-1. However, the results of subsequent mechanistic, pre-steady state and full progress kinetic experiments are consistent with a mechanism in which an enamine forms between Pro-1 and the allene. Hydrolysis of the enamine or an imine tautomer produces acetoacetate. Reduction of the imine species is likely responsible for the observed enzyme inactivation. This is the first reported observation of a tautomerase superfamily member functioning by covalent catalysis. The results may suggest that some fraction of the *cis*-CaaD-catalyzed dehalogenation of *cis*-3-haloacrylates also proceeds by covalent catalysis.

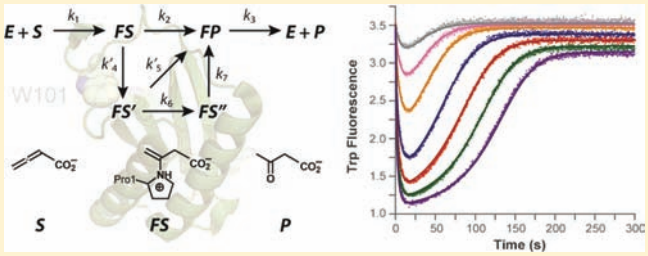

1. INTRODUCTION

cis-3-Chloroacrylic acid dehalogenase (*cis*-CaaD) catalyzes the hydrolytic dehalogenation of *cis*-3-chloroacrylate (**2**, Scheme 1)

Scheme 1

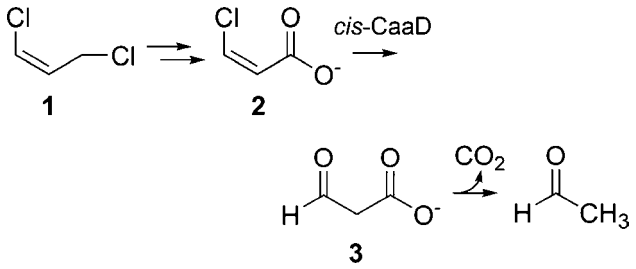

to afford malonate semialdehyde (**3**).[1−5] The reaction is part of a bacterial catabolic pathway for the *cis*-isomer of 1,3-dichloropropene (**1**), which, along with the *trans*-isomer make up the active components of the nematocide marketed as Telone II and Shell D-D.[1−5] The subsequent decarboxylation of **3** produces acetaldehyde and completes the overall conversion of **1** into a compound that can feed into the Krebs cycle.[1−5]

The enzyme is a tautomerase superfamily member and exhibits the characteristic $\beta-\alpha-\beta$ fold and catalytic amino-terminal proline.[6,7] On the basis of this superfamily categorization,[8,9] sequence analysis,[1,2,6] crystallographic[10,11] and mutagenic studies,[12,13] pre-steady state[14] and steady state kinetic analysis,[8,14] and the characterization of its reactions with inhibitors and substrate analogues,[1,12] a working hypothesis for the mechanism (Scheme 2) has been formulated. In this mechanism, Glu-114 and Tyr-103 function to activate a water molecule for addition to C-3 of **2**. A triad of amino acid residues (His-28, Arg-70, and Arg-73) interacts with the C-1 carboxylate group in an unknown manner, and through this interaction likely binds and polarizes the substrate. Polarization creates a partial positive charge at C-3, which facilitates the addition of water. The resulting enediolate **4**, can collapse to pick up a proton at C-2 (from Pro-1, functioning as a general acid), and produce the chlorohydrin **5** (Scheme 2, path A). Expulsion of the chloride results in **3**. Alternatively, the enediolate **4** can undergo an α,β-elimination of HCl to yield enol **6**, which ketonizes to generate **3** (Scheme 2, path B).

cis-CaaD processes other substrates including the allene species, 2,3-butadienoate (**7**, Scheme 3A). The mechanism for the dehalogenation of **2** suggests that *cis*-CaaD adds water across the 2,3 double bond of **7** to produce an enol species, which can ketonize and pick up a proton at C-4 to generate the final product, acetoactetate (**8**). The allene and substituted derivatives are of interest because they can be used as

Received: July 22, 2011
Published: November 30, 2011

Scheme 2

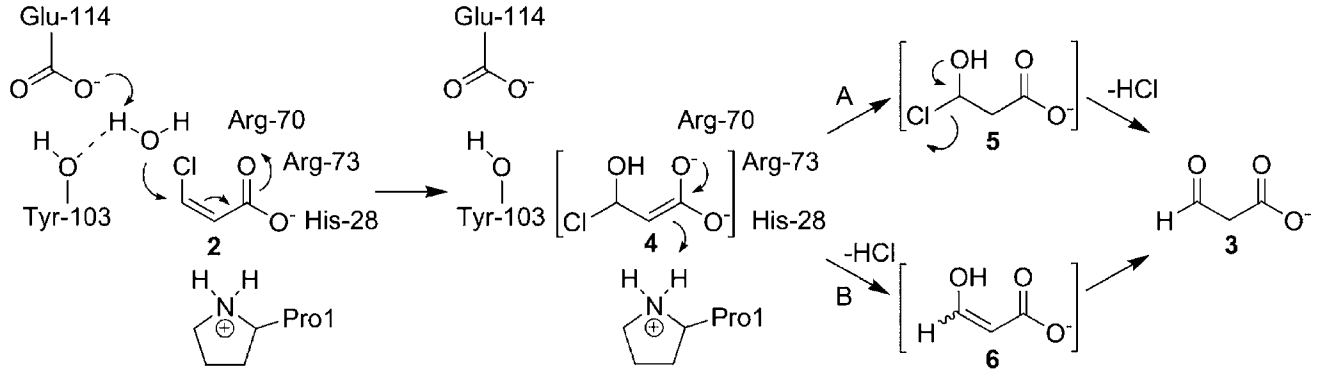

Scheme 3

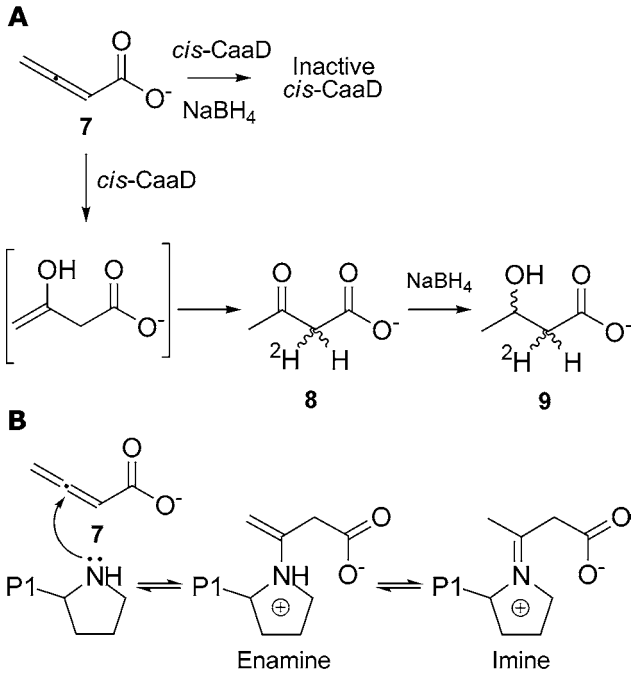

stereochemical probes of the hydration reaction that enable us to infer the overall stereochemical course (*syn* vs *anti*) for the reaction using **2**. The stereochemical course narrows the mechanistic possibilities and indicates the positions of the active site residues relative to the substrate.

As a first step in this stereochemical analysis, *cis*-CaaD was incubated with **7** in ^2H_2O in the presence of $NaBH_4$ (Scheme 3A). It was anticipated that the configuration at C-2 of [2-^{2}H]**8** would be fixed by its immediate reduction to [2-^{2}H]-3-hydroxybutyrate (**9**). Unexpectedly, this strategy did not generate [2-^{2}H]**9**, but instead, resulted in *cis*-CaaD inactivation. This observation prompted an in-depth mechanistic and kinetic examination of the reaction between *cis*-CaaD and **7**. Possible mechanistic scenarios for the enzyme-catalyzed hydration of **7** and enzyme inactivation in the presence of **7** and $NaBH_4$ are evaluated in light of the results. Both mechanisms are initiated by the nucleophilic attack of the prolyl nitrogen of Pro-1 at C-3 of **7** to form an enamine (Scheme 3B). Hydrolysis of the enamine or the imine tautomer could produce **8**, whereas inactivation likely occurs by the reduction of the imine tautomer. Although the allene is not a known biological substrate for *cis*-CaaD, this is the first report of a tautomerase superfamily processing a substrate through a covalent intermediate. The implications of this observation for the *cis*-CaaD-catalyzed transformation of **2** are discussed.

2. MATERIALS AND METHODS

Chemicals, biochemicals, Luria–Bertani (LB) medium components, solvents, and molecular biology reagents were obtained from sources reported elsewhere.[1,15] 2,3-Butadienoate (**7**) was synthesized according to published methods.[16] 2-Hydroxy-2,4-pentadienoate (**10**) was synthesized and purified as described previously.[17,18] *cis*-CaaD, acetoacetate decarboxylase (AAD), and the 4-oxalocrotonate decarboxylase/vinylpyruvate hydratase complex (4-OD/VPH) were expressed and purified according to previously described protocols.[1,18,19] D-*β*-Hydroxybutyrate dehydrogenase (*β*-HBD) from *Pseudomonas lemoignei*, sequencing grade endoproteinase Glu-C (protease V-8) from *Staphylococcus aureus*, fully protio (3*S*)-**9**, and **2** were purchased from Sigma-Aldrich Chemical Co. (St. Louis, MO). Gravity flow chromatography columns (Econo-Column) and Dowex AG-X8 resin (formate form, 200–400 mesh) were obtained from BioRad (Hercules, CA). DEAE-Sepharose and Phenyl-Sepharose 6 Fast Flow resins were acquired from Sigma-Aldrich Chemical Co. Amicon stirred cell concentrators and ultrafiltration membranes (3000 MW cutoff) were purchased from Millipore Corp. (Billerica, MA).

Positive ion mode mass spectral (MS) data were collected in the Institute for Cellular and Molecular Biology Protein and Metabolite Analysis Facility at the University of Texas at Austin. An LCQ electrospray ion-trap (ESI) mass spectrometer (Thermo, San Jose, CA) was used for protein mass identification and a Voyager-DE Pro matrix-assisted laser desorption/ionization (MALDI) mass spectrometer (PerSeptive Biosystems, Framingham, MA) was used to determine peptide masses. Negative ion mode MS data were collected in the Laboratory for Biological Mass Spectrometry (Department of Chemistry, Texas A&M University, College Station, TX) on a PE Sciex APJ Qstar Pulsar ESI-mass spectrometer. Nuclear magnetic resonance (NMR) spectra were recorded on a Varian INOVA-500 spectrometer (Palo Alto, CA). Unless otherwise indicated, the lock signal is ^2H_2O. NMR signals were analyzed using the software program SpinWorks 3.1.6 (Copyright 2009 Kirk Marat, University of Manitoba). Steady state kinetic assays were performed on an Agilent 8453 diode-array spectrophotometer at 22 °C. Nonlinear regression analysis was performed using the program Grafit (Erithacus Software Ltd., Staines, U.K.). Protein concentrations were determined by the Waddell method.[20]

Generation and Stereochemical Analysis of [2-^{2}H]8. The stereochemical analysis of [2-^{2}H]**8** was carried out by the series of reactions shown in Scheme 4A. The enzyme *cis*-CaaD (0.6 mM) was exchanged into ^2H_2O (20 mM $Na_2{}^2HPO_4$ buffer made up in ^2H_2O, pH 7.2) using an Amicon concentrator (3000 MW cutoff). In order to exchange the carboxylic acid proton of **7** (20 mg, 0.28 mmol) with a deuteron, it was initially dissolved in deuteriated methanol (500 μL) and rotary evaporated to dryness. This process was repeated 3 times. The exchanged sample (**7**) was then reconstituted in anhydrous

dx.doi.org/10.1021/ja206873f | J. Am. Chem.Soc. 2012, 134, 293–304

Scheme 4

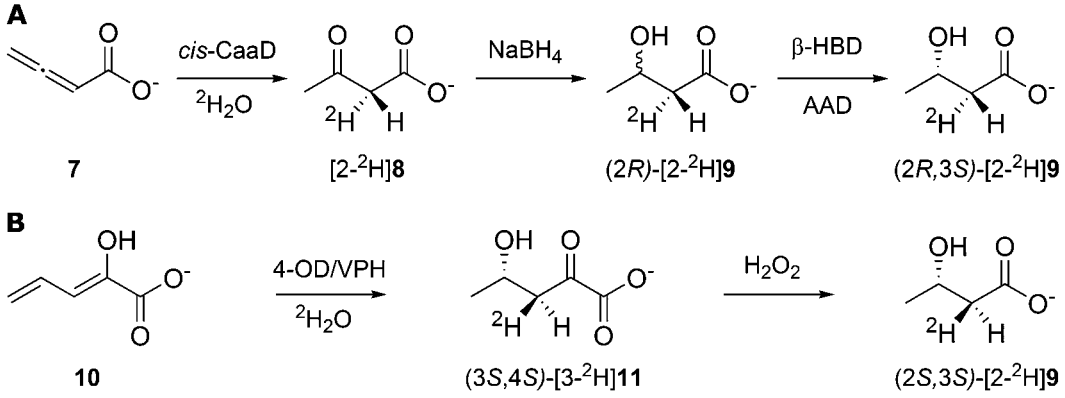

DMSO-d_6 (150 μL). A total of 30 μL of this solution was then added to 0.6 mL of 100 mM $Na_2{}^2HPO_4$ buffer made up in ^2H_2O, and immediately mixed with a previously exchanged solution of *cis*-CaaD (40 μL of a 0.6 mM solution). A total of five reaction mixtures were made. After 5 min, the reaction mixtures were treated with $NaBH_4$ (100 μL of a 2.6 M solution made up in ^2H_2O). The reaction mixtures were combined after sitting overnight and the pH of the solution was adjusted to ~4.5 with 8.5% phosphoric acid. The mixture was allowed to stand at room temperature until bubbling ceased. The pH was then adjusted to ~8 with 1 M NaOH, and the mixture containing [2-^{2}H]**9** was subjected to anion-exchange chromatography on a Dowex AG-X8 (formate) column, using a linear gradient (0−2 M aqueous formic acid, 200 mL). Compound **9** (6.8 mg, 0.065 mmol) eluted between 0.3 and 0.5 M formic acid. The combined fractions were evaporated to dryness, the residue was dissolved in 5 mL of 20 mM Na_2HPO_4 buffer, NAD^+ (0.6 equiv) was added, and the pH was adjusted to 7.8 with 1 M NaOH. The (3*R*)-isomer of [2-^{2}H]**9** was removed by treating the resulting solution with D-*β*-hydroxybutyrate dehydrogenase (D-*β*-HBD, 100 μL aliquot of a 0.05 units/μL solution in 20 mM Na_2HPO_4 buffer, pH 7.8) and acetoacetate decarboxylase (AAD, a 100 μL aliquot of crude protein extract from 1 g of cells in 20 mM Na_2HPO_4 buffer pH 7.8).[19] After standing at room temperature for 24 h, the pH was adjusted to 8 with 1 M NaOH and the remaining (3*S*)-[2-^{2}H]**9** (2.4 mg, 0.023 mmol) was isolated as described above using anion-exchange chromatography. The appropriate fractions were combined, evaporated to dryness, dissolved in 100 mM $Na_2{}^2HPO_4$ buffer (600 μL) made up in ^2H_2O (pH 7.87), and analyzed by ^{1}H NMR spectroscopy. ^{1}H NMR (^2H_2O, 500 MHz) δ 1.06 (~2.2 H, brd d, C^{2}HH$_2$ at C-4), 2.16 (~0.8 H, brd d, CH at C-2), 2.26 (~0.2 H, brd d, CH at C-2), 4.01 (1H, q, CH at C3).

Generation of (2*S*,3*S*)-[2-^{2}H]9. A configurationally known sample of (2*S*,3*S*)-[2-^{2}H]**9** was generated by the series of reactions shown in Scheme 4B.[17,18] Accordingly, 2-hydroxy-2,4-pentadienoate (**10**, 4 mg, 0.035 mmol), previously exchanged with deuteriated methanol as described above for **7**, was dissolved in anhydrous DMSO-d_6 (30 μL) and added to 600 μL of 100 mM $Na_2{}^2HPO_4$ buffer made up in ^2H_2O. A 100 μL aliquot of a 4-OD/VPH solution (crude protein extract from 1 g of cells) was added to the mixture. The enzyme solution had previously been exchanged into 20 mM $Na_2{}^2HPO_4$ buffer (containing 5 mM $MgCl_2$) made up in ^2H_2O (pH 7.2). After standing at room temperature for 5 min, stereospecifically generating [3-^{2}H]**11**, the reaction mixture was treated with enough 30% H_2O_2 solution to make a 3% H_2O_2 solution by volume. After 1.5 h, catalase (150 units in 5 μL) was added. The pH was adjusted to 8 after bubbling ceased, and the labeled product (2*S*,3*S*)-[2-^{2}H]**9** was isolated as described above by anion-exchange chromatography and analyzed by ^{1}H NMR spectroscopy. ^{1}H NMR (^2H_2O, 500 MHz) δ 1.06 (~1.5 H, brd d, C^{2}HH$_2$ at C-4), 2.26 (1 H, brd d, CH at C-2), 4.01 (1H, q, CH at C3). For comparison, a ^{1}H NMR spectrum was recorded in ^2H_2O using fully protio (3*S*)-**9**.

ESI-MS Analysis of $NaCNBH_3$-Treated Mixtures Containing *cis*-CaaD and 7, 8, or Acetone. Four reaction mixtures (250 μL) were made up containing 100 mM Na_2HPO_4 buffer (175 μL, pH ~8.0), $NaCNBH_3$ (50 μL of a 1.6 M solution in 100 mM Na_2HPO_4 buffer, pH ~9.5) and *cis*-CaaD (25 μL of a 1.2 mM solution in 100 mM Na_2HPO_4 buffer, pH 8). After a 10-min incubation, **7** (0.5 mg, 0.007 mmol), **8** (5 mg, 0.05 mmol), or acetone (0.5 mg, 0.0086 mmol) was added to the reaction mixture. The fourth reaction mixture served as a control. An additional reaction mixture was made up similarly, but contained **8** (5 mg, 0.05 mmol) and $NaBH_4$ (5 mg, 0.13 mmol). Reaction mixtures were incubated for at least 30 min, except for the sample containing acetone, which was allowed to incubate for 24 h. Residual *cis*-CaaD activity in each mixture was determined by the steady state UV assay described below using **2** (0.5 mM). The individual samples were desalted on a PD-10 Sephadex G-25 gel filtration column prewashed with 50 mL of 10 mM NH_4HCO_3 buffer (pH ~8). After loading the sample, each column was washed with an additional 5 mL of NH_4HCO_3 buffer. The fractions (0.3 mL) were screened for protein using the Bradford reagent.[21] The enzyme typically eluted in fractions 8−12. The protein concentrations of the fractions containing the most protein (as assessed by the Bradford reagent) were quantified by the Waddell method.[20] Aliquots of the fractions containing *cis*-CaaD were analyzed by ESI-MS.

Peptide Mapping and MALDI-MS Analysis. Unmodified *cis*-CaaD (~35 μg) or modified *cis*-CaaD (~13 μg), prepared above by incubating *cis*-CaaD, **7**, and $NaCNBH_3$, was placed in 27 μL of 100 mM Na_2HPO_4 buffer (pH 8) containing 1 M guanidine hydrochloride, and mixed with 3 μL (0.75 μg) of sequencing grade protease V-8 (8.6 μM in 100 mM Na_2HPO_4 buffer, pH 8).[22] The protein samples were incubated overnight at 37 °C and the resulting peptide mixture was prepared and analyzed by MALDI-MS, as described previously.[12,15]

^{1}H NMR Spectroscopic Monitoring of an Incubation Mixture Containing *cis*-CaaD and 8. A reaction mixture containing *cis*-CaaD and authentic **8** was monitored by ^{1}H NMR spectroscopy for acetone production. Acetone could result from the decarboxylation of an imine adduct formed in the course of the reaction of **7** and *cis*-CaaD (Scheme 3B), and the subsequent hydrolysis of the resulting acetone imine.[23] Accordingly, **8** (4 mg, 0.04 mmol) was added to 100 mM Na_2HPO_4 buffer (pH 9.2, 600 μL) containing 30 μL of DMSO-d_6. Subsequently, a 25 μL aliquot of *cis*-CaaD (from a 1.2 mM stock solution) was added to the sample and the mixture was incubated for 24 h prior to analysis by ^{1}H NMR spectroscopy. A control sample was prepared in a like manner, but a 25 μL aliquot of buffer was added rather than enzyme. The NMR spectra were recorded on a Varian INOVA-500 spectrometer (Palo Alto, CA) using selective presaturation of the water signal with a 2 s presaturation interval. The lock signal is DMSO-d_6. Chemical shifts are standardized to the DMSO-d_6 signal at 2.49 ppm.

Irreversible Inhibition of *cis*-CaaD in the Presence of 7 and $NaCNBH_3$. The reaction mixtures contained $NaCNBH_3$ (25 μL of a 3.2 M stock solution in 100 mM Na_2HPO_4 buffer, pH 8) and varying amounts of **7** (0−90 μL from a 6.1 mM stock solution made up in 100 mM Na_2HPO_4 buffer, pH 8) for a total volume of 150 μL. The reactions were initiated by the addition of a 150 μL aliquot of a 1.2

dx.doi.org/10.1021/ja206873f | J. Am. Chem.Soc. 2012, 134, 293−304

mM solution of *cis*-CaaD (3 mg total) in 100 mM Na_2HPO_4 buffer (pH 8). After an overnight incubation period to ensure reaction completion, the remaining *cis*-CaaD activity was measured using **2**, as follows and described elsewhere.[1] The assay mixtures (1 mL) contained 5 μL of the incubation mixture and 10 μL of **2** (100 mM) in 100 mM Na_2HPO_4 buffer (pH 8, where *cis*-CaaD exhibits optimal activity with **2**, as assessed by k_{cat}[12]). The loss of substrate was monitored at 224 nm (ε = 3600 M^{-1} cm^{-1}) for increasing time periods (1−15 min), depending on the concentration of **7**. Initial rates were determined in triplicate from linear fits to the UV data. The % activity was then plotted versus the number of equivalents of **7** (per trimer). The data was fit to a modified form of the quadratic equation (Text S1 in Supporting Information [SI]), with the assumption of infinitely tight binding (i.e., irreversible inhibition), to estimate the number of equivalents of **7** required for complete inhibition. The experiment was repeated using a *cis*-CaaD concentration of 4 mg (total) and the appropriate adjustments in the number of equivalents of **7**.

Pre-steady State Kinetics. All experiments were conducted on a SF 2004 series stopped-flow apparatus (KinTek Corp, Austin, TX) at 22 °C. Enzyme fluorescence (Trp-101)[14] was monitored for 0.2, 1, 20, or 300 s with excitation at 280 nm. The monochromator slit widths were set at 0.28 mm, and emission was observed using a 340 nm band-pass filter (Semrock, Rochester, NY). Fluorescent traces for the 0.2, 1, or 20 s data represent an average of at least 5 individual runs (1000 data points each). Fluorescent traces for the 300 s data represent single runs (1000 data points each) with slit widths set at 0.12 mm. For a typical experiment, enzyme (0.02 mM before mixing, equilibrated 1 h) and a solution of **7** (0−16 mM before mixing) or **8** (0−20 mM before mixing) were mixed in a 1:1 ratio in the stopped-flow instrument (1.3 ms dead time). All solutions were made up in 100 mM Na_2HPO_4 buffer at pH 8.0.

Steady State and Full Time Course Kinetics with *cis*-CaaD and 7. Assays (1 mL) were carried out in 100 mM Na_2HPO_4 buffer at pH 8.0. Enzyme solution stocks (~1 mM) were diluted to 2 μM (monomer mass) and allowed to equilibrate for at least 1 h at 22 °C prior to use. Assays were initiated by the addition of 0.25−20 μL of **7** (50 mM stock solution in 100 mM Na_2HPO_4 buffer, pH 8) to final concentrations of 25−1000 μM. The loss in UV absorbance was followed at 224 nm (ε = 1125 $M^{-1}cm^{-1}$) for 40 s (1.5 s cycle time) with initial rates estimated from the first 16 s of reaction. The steady state parameters k_{cat} and K_m were determined by nonlinear regression using the Michaelis−Menten equation. The reaction time course (224 nm) was monitored for 300 s at two substrate concentrations (150 and 250 μM) for use in the global fitting analysis (see below).

The reaction was also followed to completion (300 s) at 280 nm (10 μM enzyme, monomer mass) with various concentrations of **7** (1080, 2160, 3240, 4320, 5400 μM). The corresponding time-resolved spectra (240−330 nm) for two concentrations (2160 and 4320 μM) were deconvoluted using singular value decomposition (SVD, SpectraFit feature of KinTek Explorer), to resolve the relative contributions of **7** (ε_{280} = 8.8 M^{-1} cm^{-1}), **8**, (ε_{280} = 45 M^{-1} cm^{-1}), and an intermediate as a function of time. Controls with enzyme or product alone were carried out.

Data and Global Fitting Analysis. All of the stopped-flow, steady state, full time course, and time-resolved spectra data were fit by simulation to a single kinetic model using the computer program KinTek Explorer. This program simulates experimental results by using direct numerical integration of rate equations for the full model,[24] yielding estimates for the rate constants of kinetically significant steps. As an additional constraint, the steady state value for k_{cat}/K_m (for **7**) provided an estimate for the lower limit on the second order rate constant k_1. The KinTek program FitSpace was used to evaluate the uniqueness of a particular fit to the data and to provide more realistic error estimates for the fitted rate constants.[25] A more detailed description of FitSpace can be found in the SI and elsewhere.[25]

Deconvolution of time-resolved spectra with the SVD function of KinTek Explorer produces eigenvectors for each significantly contributing species and a corresponding amplitude as a function of time. Assignment of each set of amplitude data to the simulated concentrations of individual species (derived during the global fitting) allows resolution of the actual time dependence and spectra of each species. As a final check, the time-resolved spectra were reconstituted as the product of the spectra and time dependence of each species.

Fitting of the stopped-flow data also incorporated a term to account for fluorescence signal reduction due to absorption of excitation radiation (280 nm) by various species as a function of time. The reduction in incident light intensity (I) is a logarithmic function ($I = I_{ref}10^{-\varepsilon cl}$) dependent on the extinction coefficient (ε) and concentration (c) of the absorbing species and the cell path length (l = 0.5 cm). However, as observed fluorescence is the sum of light from the full path length of the cell, the average light intensity across the window (approximated by $l/2$, see SI Text S2) was used. The simulated fluorescence signal (Text S2 and eq S2 of SI) was therefore multiplied by the factor $10^{-d(l/2)}$, where d represents the sum of the simulated concentrations of **7**, **8** and the intermediate multiplied by their respective extinction coefficients. The value of ε_{280} for the intermediate was determined by global fitting.

3. RESULTS

Assignment of the Stereochemistry at C-2 of [2-^{2}H]8.

The stereochemical analysis of [2-^{2}H]**8**, generated by the *cis*-CaaD-catalyzed hydration of **7** in ^2H_2O, was carried out by its chemical and enzymatic degradation to (2*R*,3*S*)-[2-^{2}H]**9** (Scheme 4A). A comparison of the ^{1}H NMR spectrum to that of an authentic sample established the stereochemistry. In our initial strategy, $NaBH_4$ was included in the reaction mixture to minimize the nonenzymatic deuteron incorporation at C-2 (of **8**) and loss of chirality. This approach resulted in the enzyme's inactivation without producing detectable quantities of [2-^{2}H]**9**. Hence, *cis*-CaaD and **7** were allowed to react for 5 min before the addition of $NaBH_4$. This strategy was successful and also produced both the 3*R* and 3*S* isomers of [2-^{2}H]**9** because the $NaBH_4$ reduction of [2-^{2}H]**8** is stereorandom. Incubation of the mixture with D-β-hydroxybutyrate dehydrogenase, NAD^+, and acetoacetate decarboxylase (AAD)[19] removed the 3*R*-isomer by the oxidation (at C-3) and decarboxylation of the resulting acetoacetate. Decarboxylation of acetoacetate ensures reaction completion. Purification by anion-exchange chromatography affords the 3*S*-isomer of the C-2 monodeuteriated **9**.

The diastereotopic C-2 protons of the fully protio (3*S*)-**9** each appear as a doublet of doublets centered at 2.17 ppm and 2.28 ppm in a ^{1}H NMR spectrum (Figure 1A).[17,18] The

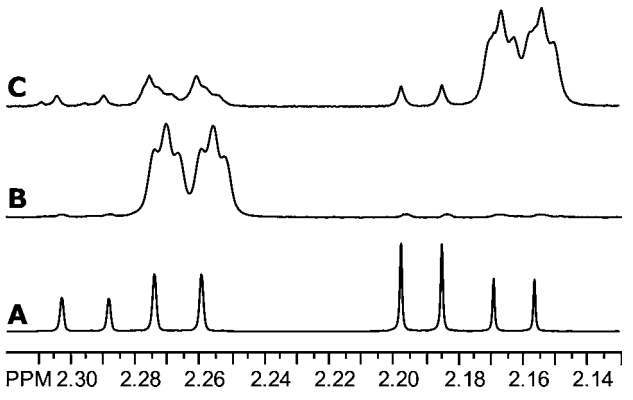

Figure 1. ^{1}H NMR spectrum (500 MHz) in ^2H_2O of (A) fully protio (3*S*)-**9**, (B) (2*S*,3*S*)-[2-^{2}H]**9** generated from the 4OD/VPH-catalyzed reaction of **10** and subsequent degradation, as reported in the text, and (C) (2*R*,3*S*)-[2-^{2}H]**9** derived from the *cis*-CaaD-catalyzed hydration of **7** in ^2H_2O, as reported in the text.

stereospecific incorporation of a deuteron leads to the loss of the upfield signal (2.17 ppm) and a collapse of the other signal (2.28 ppm) into a broadened doublet, as observed in the spectrum for a sample of (2*S*,3*S*)-[2-^{2}H]**9** (Figure 1B).[18] This sample was generated by the enzymatic and chemical conversion of **10** to (2*S*,3*S*)-[2-^{2}H]**9** in ^2H_2O (Scheme 4B). The 4-OD/VPH complex converts **10** to 2-oxo-(4*S*)-hydroxypentanote (**11**).[17,18] In ^2H_2O, it has previously been established that this complex produces (3*S*)-[3-^{2}H]**11** in a stereospecific manner.[17,18] Treatment of (3*S*)-[3-^{2}H]**11** with H_2O_2 results in oxidative decarboxylation and yields (2*S*,3*S*)-[2-^{2}H]**9**.

The ^{1}H NMR spectrum of the isolated (3*S*)-[2-^{2}H]**9** shows two major signals for the protons at C2, both are broadened doublets centered at 2.16 ppm and 2.26 ppm (Figure 1C). The integral of one signal (2.16 ppm) is favored over the other one by a factor of 5:1, indicating that the reaction was stereoselective. The upfield doublet predominates, indicating that (2*R*,3*S*)-[2-^{2}H]**9** is the major isomer recovered. This observation indicates that the stereochemistry at C-2 of **8** is *R*. The amount of proton scrambling observed in the product (~20%) is most likely due to the nonenzymatic deuteron incorporation at C-2. The small amounts of the fully protio compound observed in the spectra shown in B and C of Figure 1 are likely due to residual H_2O in the reaction mixtures.

$NaCNBH_3$ Trapping Experiments and ESI-MS Analysis. The observed inactivation of *cis*-CaaD in the presence of **7** and $NaBH_4$ suggested a mechanism initiated by the nucleophilic attack of the prolyl nitrogen of Pro-1 at C-3 of **7** to yield an enamine (Scheme 3B). The enamine equilibrates with an imine tautomer, which can be reduced by $NaBH_4$ or $NaCNBH_3$ (Scheme 3B). The ESI mass spectra for the unmodified and modified *cis*-CaaD, recovered from a trapping experiment (using $NaCNBH_3$ at pH 8) of a mixture of *cis*-CaaD and **7**, are shown in Figure 2. The molecular mass of *cis*-CaaD

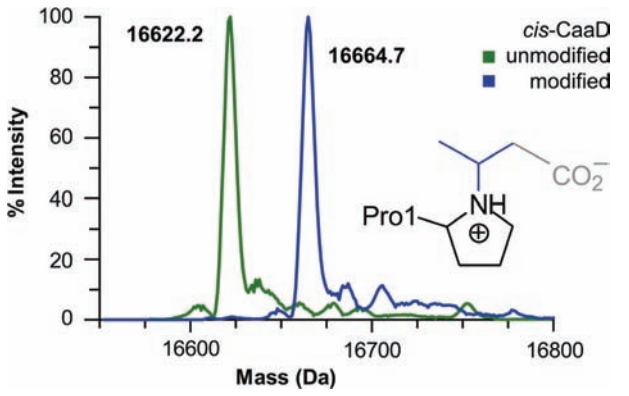

Figure 2. ESI-MS spectrum of wild-type *cis*-CaaD incubated with $NaCNBH_3$ at pH 8 in the absence (green) or presence (blue) of **7**. The signal at 16,622.2 corresponds to the unmodified enzyme, as described in the text. The signal at 16,664.7 Da corresponds to the modified enzyme, as described in the text.

(green) is 16,622.2 Da, within experimental error of the calculated mass (16,624 Da).[14] The molecular mass of the modified *cis*-CaaD (blue) is 16,664.7 Da, which represents nearly 100% modification of the enzyme. The difference in mass from that of the control sample is 42.5 Da, which is consistent with the mass of a decarboxylated, reduced imine of **7** (43.1 Da, see Figure 2 for structure). Results from negative ion mode MS analysis are the same (data not shown). Different amounts of the decarboxylated product were also observed as a function of the ESI-MS conditions (e.g., direct infusion or liquid chromatography/MS), as previously reported.[15]

The possible inactivation of *cis*-CaaD by **8** or acetone in the presence of $NaCNBH_3$ or $NaBH_4$ was examined. Acetone could result from the decarboxylation of **8** in an enzymatic or nonenzymatic process. It was not possible to trap a covalently modified *cis*-CaaD under any of these experimental conditions (Figure S1, SI) nor was any irreversible inhibition (using **2**) observed by activity assays. Furthermore, *cis*-CaaD did not catalyze the decarboxylation of **8** to acetone. ^{1}H NMR analysis indicated that incubated samples (16 h) of **8**, alone, or with *cis*-CaaD contained equivalent, but small, amounts of acetone (Figure S2A,B, SI).[26] The sum of these observations argues against Schiff base formation between *cis*-CaaD and **8** or acetone, and subsequent reduction, as the cause of *cis*-CaaD inactivation.

Peptide Mapping and MALDI-MS Analysis. The *cis*-CaaD samples (unmodified and modified) were treated with endoproteinase Glu-C (protease V-8) and the resulting peptide mixtures were analyzed by MALDI-MS in order to identify the site of covalent modification on *cis*-CaaD. Protease V-8 hydrolyzes peptides at the carboxylate side of glutamate and aspartate residues.[22] The spectrum for the modified *cis*-CaaD (recovered from the $NaCNBH_3$ treatment of a mixture of *cis*-CaaD and **7**) is shown in Figure S3 (SI). The spectrum shows two signals in the region of interest: the minor signal corresponds to the unmodified peptide Pro-1-Asp-26 (2860.8 Da), as previously reported,[12] and the major signal corresponds to the same peptide modified after incubation with **7** (2902.8 Da).[27] The mass difference between the two peaks is 42 Da, which is consistent with the calculated addition of the decarboxylated and reduced imine of **7** (43.1 Da).

***cis*-CaaD Inhibition by 7 in the presence of $NaCNBH_3$.** *cis*-CaaD (3 mg) was incubated with **7** in the presence of $NaCNBH_3$ in order to determine the number of equivalents of **7** required to inactivate the enzyme. The % activity decreases as a function of increasing equivalents of **7** per trimer (Figure 3). The data fit satisfactorily to a modified

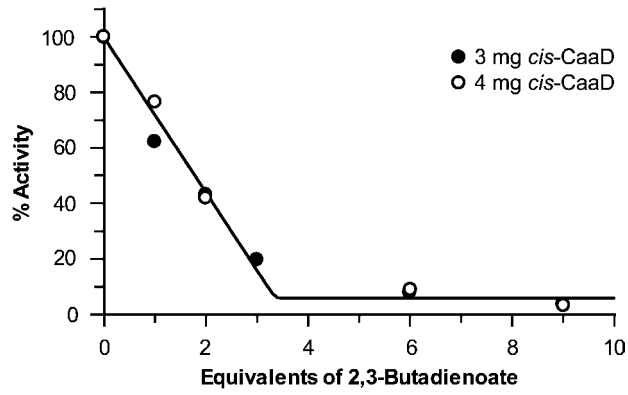

Figure 3. Plot of *cis*-CaaD activity (%) remaining as a function of increasing concentration of **7** in the presence of $NaCNBH_3$ at pH 8. The solid line is a fit of the data to a modified form of the quadratic equation (see text and SI, Text S1).

form of the quadratic equation (eq S1 in SI) which assumes infinitely tight (irreversible) binding allowing the end point to float during the data fitting (giving a background of ~6%). The

dx.doi.org/10.1021/ja206873f | J. Am. Chem.Soc. 2012, 134, 293–304

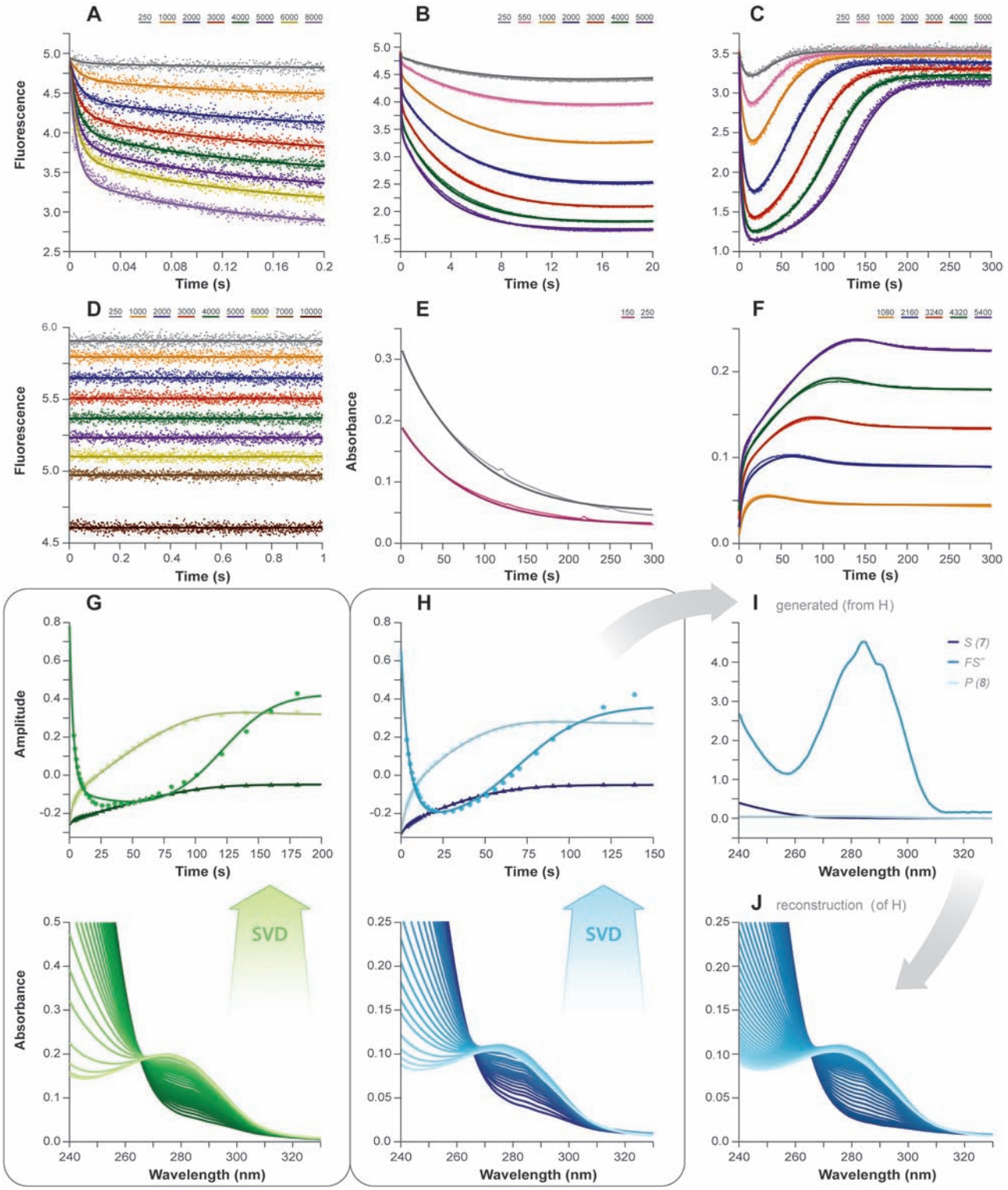

Figure 4. *cis*-CaaD kinetic data with **7** and **8** globally fit by simulation (A–H) to the mechanism in Scheme 6 (solid lines). Initial concentrations (after mixing) are reported in μM and colored according to the figure keys. (A–C) Stopped-flow fluorescence traces recorded at 250–8000 μM of **7** (0.2, 20, and 300 s, respectively) and enzyme (10 μM). (D) Stopped-flow fluorescence traces recorded at 250–10000 μM of **8** and enzyme (10 μM). (E,F) Full time course kinetic traces following decrease at 224 nm (2 μM enzyme) and increase at 280 nm (10 μM enzyme), respectively, using 100–250 and 1080–5400 μM of **7**. (G,H) Amplitude eigenvectors (upper panels) isolated by singular value decomposition (SVD) from the corresponding time-resolved spectra (lower panels, 4130 and 2160 μM **7**, respectively). (I) Spectra for **7** (dark blue), intermediate FS″ (teal, largest peak) and **8** (light blue), generated from the global fit shown in H, upper panel. The *y*-axis corresponds to the extinction coefficient (mM^{-1} cm^{-1}). (J) Reconstruction (0–150 s) of actual time-resolved spectra shown in H (1.4–150 s), lower panel.

number of equivalents of **7** required for complete inhibition (and covalent modification of each Pro-1) estimated by this analysis (SI, Text S1) was 3.4 ± 0.2 equiv per trimer. The results with a higher enzyme concentration (4 mg, open circles)

dx.doi.org/10.1021/ja206873f | *J. Am. Chem.Soc.* 2012, 134, 293–304

were the same (3.4 equiv). These results are consistent with the exclusive direct attack of 7 by Pro-1 as the first step of the reaction after binding.

Pre-steady State Kinetics. Pre-steady state stopped-flow fluorescence experiments were conducted to evaluate proposed mechanisms for the reaction of *cis*-CaaD and 7. All of the steady state and pre-steady data shown in Figure 4 were globally fit to a single, unifying model based upon simulation (KinTek Explorer) to resolve the individual rate constants for each of the kinetically distinguishable steps. The stopped-flow fluorescence traces (0.2, 1, 20, and 300 s) are shown in Figure 4A, 4SA (SI), and 4B,C, respectively, along with the corresponding global fits by simulation (solid lines). The traces exhibit an initial fluorescence drop during the dead time of the instrument (1.3 ms), the amplitude of which increases linearly with increasing substrate concentration (SI, Figure S5A,B). This drop is followed by a rapid loss in fluorescence, and then a slower decrease in fluorescence intensity (Figure 4A), which can be approximated by a double exponential. This is followed by a slow increase in the fluorescence signal (after ~20 s), which eventually reaches a plateau, signifying reaction completion (300 s, Figure 4C). The end point fluorescence plateau in the 300 s data set decreases as a function of increasing substrate concentration, rather than returning to the initial fluorescence value for free enzyme alone (Figure 4C). Moreover, this drop in fluorescence intensity occurs with a concomitant increase in the absorbance at 280 nm (*vida infra*).

It should be noted that the kinetics are quite complex and the system never reaches an extended steady state phase. Rather the concentrations of enzyme-bound species, as reflected by changes in fluorescence emission, are changing constantly. Attempts to fit the data by conventional means, using sums of exponential functions, failed to achieve an adequate representation of the data. Therefore, we have fit the entire data set based upon a minimal model and numerical integration of the rate equations. For this endeavor to succeed it is necessary to include every component of the reaction mixtures, including the effects of the products of the reaction on enzyme turnover and the absorption of incident light.

We examined the effect of the reaction product by stopped-flow fluorescence experiments (1 s) by mixing enzyme and **8** to get the results shown in Figure 4D. The traces (neglecting the dead time of the instrument, 1.3 ms) are time independent over this range and the change in fluorescence exhibits a linear decrease (R^2 = 0.99) with increasing concentration of **8**. The *cis*-CaaD-catalyzed conversion of 7 to **8** (over 300 s) exhibits a decrease in absorbance when monitored at 224 nm (Figure 4E) and an increase in absorbance when monitored at 280 nm (Figure 4F). In view of these observations, it is reasonable to propose that the observed instantaneous drop in the fluorescence signal for the reaction of enzyme and **8** (i.e., Figure 4D) corresponds to the absorbance of the excitation radiation (280 nm) due to the enol form of **8**. Therefore, these data were fit globally by simulation (Figure 4D, solid lines) using the correction factor described in the Materials and Methods and in the SI, Text S1. This approach yields an extinction coefficient of 44.3 M^{-1} cm^{-1} (authentic **8**, ε_{280} = 45 M^{-1} cm^{-1}). Moreover, a fluorescence change due to binding was not required to fit the data, which suggests that **8** binds weakly ($K_d \gg 10$ mM). This observation is consistent with the inability of **8** to covalently modify *cis*-CaaD in the presence of $NaCNBH_3$.

Steady State and Full Time Course Kinetics with *cis*-CaaD and 2 and 7. The kinetic parameters for reaction of **2** and 7 with *cis*-CaaD (determined from a conventional Michaelis–Menten analysis) are shown in Table 1. The k_{cat} values are comparable for the two substrates and the K_m value for 7 is 3-fold higher than that observed for **2**. The k_{cat}/K_m values also differ by a factor of 2.5, favoring reaction with **2**.

Table 1. Steady State Kinetic Parameters for *cis*-CaaD Catalyzed Hydration of 2 and 7[a]

	K_m (μM)	k_{cat} (s^{-1})	k_{cat}/K_m (M^{-1} s^{-1})
2	210 ± 10	4.7 ± 0.2	(2.2 ± 0.1) × 10^4
7	690 ± 30	6.0 ± 0.1	(8.7 ± 0.4) × 10^3

[a]The kinetic parameters were measured in 100 mM Na_2HPO_4 buffer (pH 8) at 22 °C following a decrease in absorbance at 224 nm. Errors are standard deviations.

The kinetic traces (300 s) following the reaction of *cis*-CaaD and 7, monitoring absorbance at 224 and 280 nm, are shown in E and F of Figure 4, respectively, along with the corresponding global fits. The kinetic traces at 280 nm exhibited a biphasic increase in absorbance (~5 s initial phase) followed by a slow decay at all concentrations of 7 (Figure 4E). The global fit to the data (solid lines) incorporated the known extinction coefficients for substrate, product and the fitted ε_{280} parameter (4400 M^{-1} cm^{-1}) for the intermediate. Control experiments conducted with **8** alone at 280 nm roughly approximated a first order decay (at a concentration of 4320 μM, k = 0.013 s^{-1} ± 0.001) and likely corresponds to the equilibrium between the enol and keto forms. The data were modeled by an equilibrium step with forward and reverse rates of 0.00085 and 0.012 s^{-1}, respectively, (Figure S4B, solid line [SI]) and incorporated into the global fit.[28]

The time-resolved spectra (240–330 nm) at concentrations of 4320 and 2160 μM of 7, respectively, are shown in the lower panels of G and H of Figure 4. Both sets of spectra exhibited a clean isosbestic point (264 nm) for the initial phase (~5 s). However, the continual increase in absorbance at ~280 nm was coupled with a slight spectral shift to higher wavelengths, followed by a decrease at ~280 nm. This observation is consistent with the formation and decay of a spectrally distinct intermediate. In order to focus the SVD analysis on the predominant reaction phase, the data (at concentrations of 4320 and 2160 μM of 7) were truncated after 200 and 150 s, respectively (see green and blue traces in C and F of Figure 4).

The SVD analysis of the time-resolved spectra shown in the lower panels of G and H of Figure 4 yielded three statistically significant eigenvectors at both concentrations of 7 (i.e., 4320 and 2160 μM), suggesting that there are three species with distinct spectra. The three corresponding amplitude eigenvectors (Figure 4G,H, upper panels) each reflect a weighted sum of substrate (7), product (**8**) and the intermediate (*FS″*, *vida infra*). Global fitting of these data according to the simulated concentration of the appropriate species, along with composite scaling factors, yield the fits (solid lines) shown in G and H (upper panels) of Figure 4. Although each eigenvector represents a weighted sum of all three species, based on the values of the scaling factors derived in fitting the data to the model, each amplitude eigenvector (to a first approximation) can be attributed as arising predominantly from a single species. This is reflected in Figure 4G,H with the amplitude eigenvectors dominated by substrate (7), product (**8**), and

dx.doi.org/10.1021/ja206873f | J. Am. Chem.Soc. 2012, 134, 293–304

the intermediate *FS″* colored dark green, light green, and green, or dark blue, light blue, and teal, respectively.[29] The individual spectra correspondingly generated for these three species, scaled by ε (mM^{-1} cm^{-1}), are shown in Figure 4I (2160 μM of **7**) and Figure S6A in SI (4320 μM of **7**). The dominant peak (λ_{max} 285 nm) corresponds to an intermediate (*FS″*, colored teal in Figure 4I) and exhibits an ε_{280} of 4500 M^{-1} cm^{-1} (2160 μM of **7**) and 4700 M^{-1} cm^{-1} (4320 μM of **7**), in good agreement with the value determined by global fitting (4400 ± 300 M^{-1} cm^{-1}). Moreover, the predicted spectra for both the substrate (**7**) and the product (**8**) are essentially identical to the experimentally observed spectra (Figure S6B in SI, 4320 μM of **7** and **8**), accurately reproducing shape, extinction coefficients, and the isosbestic point. The reconstructed time-resolved spectra (Figure S6C in SI and Figure 4J) are also nearly identical to the experimental data sets (G and H, lower panels, of Figure 4).[30]

Global Kinetic Model. The two phases observed in the initial time courses (Figure 4A and Figure S4A [SI]) are consistent with a model that has a minimum of three steps, including product release.[14,31] Steps characterized by a rapid equilibrium or those with rates significantly faster than neighboring steps (greater than 10-fold) can be difficult to resolve kinetically and may collapse into a single observable phase.[31] Therefore, a minimal model with three in-line equilibrium steps ($E + S = ES = EP = E + P$) was initially used to globally fit the data. However, no combination of rates could successfully reproduce the shape of the curves observed in the full time course stopped-flow data (e.g., Figure 4C) across the entire family of curves (250−5000 μM **7**) under conditions of limiting enzyme (10 μM). Inclusion of an additional intermediate, inferred on the basis of several lines of experimental evidence (*vida supra*), failed to account for the slow approach to steady state and simultaneously satisfy the requirements that no single step be less than k_{cat}. However, these data could be fit when the formation and decay of the additional intermediate was assigned as a branched step that was *off* the main reaction path as shown in Scheme 5 [where *E* is enzyme, *S* is substrate, (i.e., **7**), *F* is an alternate fluorescent

Scheme 5

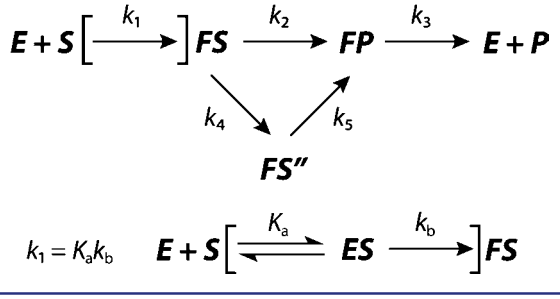

form of the enzyme with *FS″* as an intermediate and *P* is product].[32]

Model refinement, yielding Scheme 5, was based on the following observations. First, the results of the $NaCNBH_3$ trapping inhibition experiments (Figure 3) indicate that the reaction proceeds exclusively by direct attack of the prolyl nitrogen of Pro-1. In view of the reactivity of the allene, it is reasonable to propose that the formation of the initial enamine (*FS*) is irreversible. Second, the initial fluorescence drop during the dead time of the instrument suggests a fast formation of a collision complex. The linear dependence of the amplitude of the drop with substrate concentration (i.e., nonsaturating) suggests a rapid, weak binding of substrate (*ES* formation) followed by fast formation of the initial enamine (*FS*) with binding (K_a) too weak and enamine formation (k_b) too fast to measure (Figure S5A,B in SI). Therefore, we modeled this two-step process as a single kinetic step according to $E + S \rightarrow FS$ with an apparent second order rate constant $k_1 = K_a k_b$ (Scheme 5, brackets). [Further justification for this simplifying assumption and the additional evaluation of the more complex, expanded model can be found in Figure S5A−D and Text S3 in SI.] Third, the enzyme is *not* covalently modified in the presence of **8** and $NaCNBH_3$ indicating that an adduct does not form with the product. Therefore, the chemistry (hydrolysis) step (k_2, Scheme 5) was modeled as an irreversible step. Because of the lack of evidence for significant product (**8**) binding to the enzyme alone, product release was assumed to be rapid and simply modeled as an irreversible step with a fast off rate (k_3 = 2000 s^{-1}) for global fitting. The model also attributed the observed decrease in the end point fluorescence plateau as a function of increasing substrate (Figure 4C,D) to the absorbance of excitation radiation (280 nm) by product (i.e., **8**).

The global fit to the model in Scheme 5 (Table S1 in SI) could nearly account for all of the long time scale data, but could not account for an additional rapid phase in the initial time course stopped-flow data (~0.1 s, Figure S7, SI). The addition of a new species (*FS′*) was therefore required to completely fit all of the data, with the final minimal model shown in Scheme 6 (see Text S3, SI). However, during all attempts to fit the data, the values for the formation and decomposition of this new species converged to similar values. Therefore, the additional simplifying assumption that the parameters k'_4 and k'_5 are equal was incorporated into the model. Thus, we conclude that the lifetime of this additional intermediate is only sufficient to contribute to the observed

Scheme 6

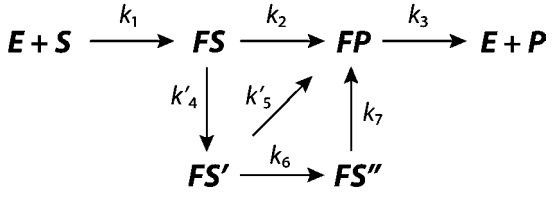

fluorescence signal during the first ~0.5 s of the enzymatic reaction.[33]

In all cases, a single fluorescence factor, representing a 4-fold quenching of fluorescence (f/f_0 = 0.26), was sufficient to describe the change in fluorescence associated with all enzyme-bound species (*F*) for the 0.2, 1, 20, and 300 s stopped-flow data (Figure 4A−C, and Figure S4A in SI). Best fit estimates for the scaling factor (f/f_0), ε_{280} for the intermediate (*FS″*), and the six rate constants from the global fit to the model shown in Scheme 6 are summarized in Table 2. The upper and lower limits were calculated using FitSpace (see SI Text S4) and reflect a threshold of 2.5% deviation from the minimal sum square error (SSE) of the best fit (error confidence contours are shown in Figure S8 of SI). The allowable variation (% range) of each best fit value was calculated by dividing the

dx.doi.org/10.1021/ja206873f | J. Am. Chem.Soc. 2012, 134, 293−304

Table 2. Rate Constants for the *cis*-CaaD Reaction with 7 Derived from the Global Fit[a]

rate	lower limit[b]	upper limit[b]	% range[c]	best fit	rate	lower limit[b]	upper limit[b]	% range[c]	best fit
f/f_0[d]	0.24	0.26	4	0.26	k'_4[f]	6.0	16.3	70	7.3 s^{-1}
ε_{280}[e]	4000	4600	8	4400 M^{-1} cm^{-1}	k'_5[f]	6.0	16.3	70	7.3 s^{-1}
k_1	7800	9000	7	8300 M^{-1} s^{-1}	k_6	1.42	1.57	5	1.42 s^{-1}
k_2	105	125	9	110 s^{-1}	k_7	0.05	0.06	10	0.052 s^{-1}

[a]The data are fit globally to the mechanism shown in Scheme 6. All steps were assumed to be irreversible with reverse rates fixed at zero during global fitting (see text). The value for k_3 was fixed at 2000 s^{-1} (see text). [b]FitSpace error confidence contours are shown in Figure S8 of SI. The upper and lower limits reflect a threshold of 2.5% deviation from the minimal SSE in the confidence contours. [c]The percentage range was calculated by dividing the mean of the range by the best fit value as (upper-lower)/(2*best fit). This reflects the allowable variation of each best fit value as a percent. [d]The fluorescence scaling factor shown as the fractional change in enzyme fluorescence (see SI, Text S2). [e]Extinction coefficient for intermediate *FS″*. [f]The fitted rate constants for k'_4 and k'_5 are the same, as these parameters were fixed at a 1:1 ratio during fitting.

mean of the range by the best fit value.[25] Overall, the model implies that three distinct enzyme-bound species are formed (in addition to enzyme−product, *FP*), each with different stabilities. The best fit value determined for k_1 ($8.3 \pm 0.6 \times 10^3$ M^{-1} s^{-1}) is within experimental error (Table 2) of the lower limit established by k_{cat}/K_m ($8.7 \pm 0.4 \times 10^3$ M^{-1} s^{-1}). Also, consistent with the only partially resolved phase describing the *FS′* species, the fitted rates for parameters k'_4 and k'_5 are not as well constrained (~70% allowable variation in the value). Moreover, it appears that the gradual build up of the *FS″* species (as indicated by the SVD analysis) and its slow decomposition rate are responsible for the shape of the curves exhibited in the full time course stopped-flow experiment (see Figure S9 of SI). This provides an indication as to why previous attempts to fit the data with an in-line mechanism failed. For such mechanisms, the value of k_{cat} provides a lower limit on any individual forward rate constant following substrate binding and proceeding through product release,[14,31] and therefore requires the decomposition rate of any intermediate to match or exceed that of k_{cat}. However, the overall full time course of the fluorescence signal is dominated by the lifetime of the relatively stable intermediate *FS″* (Figure S9 of SI), which forms and decays at a rate nearly 100-fold slower than k_{cat}. Moreover, when experiments are performed under conditions of limiting enzyme concentration relative to substrate, in-line mechanisms exhibit enzyme-bound intermediates whose concentrations are nearly invariant during an extended steady state phase, which is established after the first turnover. In contrast, our data require a change in the distribution of enzyme species on a time scale longer than a single turnover and do not exhibit an extended steady state phase, which we attribute to the slow formation and decay of off-pathway intermediates. In-line mechanisms can yield traces that appear similar to ours, but only under conditions of nearly stoichiometric enzyme:substrate ratios.[34,35] Of course, under these conditions one would not expect an extended steady state phase.

4. DISCUSSION

The inactivation of *cis*-CaaD (by covalent modification of the prolyl nitrogen) in the presence of 7 and $NaBH_4$ was initially puzzling in view of the proposed mechanism for *cis*-CaaD (Scheme 2) and the presumed mechanism for the hydration of 7 (Scheme 3A): both feature the direct hydration of substrate and not hydration by covalent catalysis. Moreover, the pK_a of the prolyl nitrogen of Pro-1 is presumed to be ~9.3 making it mostly cationic (~95%) and not nucleophilic at pH 8.0. Inactivation, however, would result from the reduction of a covalent bond between the enzyme and 7 (or a product resulting from the reaction of *cis*-CaaD and 7). We first considered the possibility that acetoacetate, **8**, the product of the enzyme-catalyzed transformation of 7, or acetone, a product resulting from the enzymatic or nonenzymatic decarboxylation of **8**, might be responsible. In such a scenario, **8** or acetone binds to the enzyme and forms a Schiff base with Pro-1. Subsequent reduction would covalently attach the compound to the enzyme via the prolyl nitrogen. Both possibilities were ruled out by three experiments: incubating the enzyme with $NaCNBH_3$ and **8** or acetone (Figure S1 of SI) does not inactivate the enzyme, the enzyme does not decarboxylate **8** to generate acetone (Figure S2 of SI), and stopped-flow fluorescence experiments indicate that **8** binds weakly or not at all (Figure 4D).

We then explored a mechanistic scenario involving the formation of a covalent bond between Pro-1 and allene 7 (Scheme 7).[36] The mechanism begins with the conjugate

Scheme 7

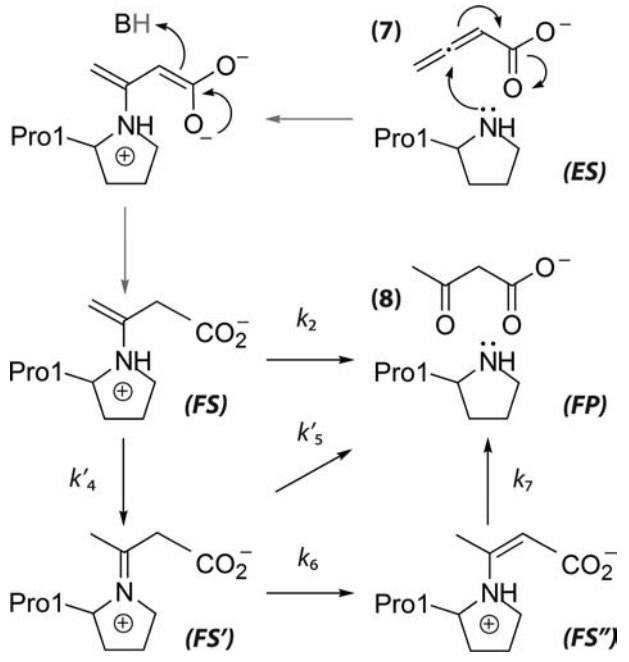

addition of the enzyme (via the prolyl nitrogen) to the 2,3 double bond of 7. The stereoselective incorporation of a proton (a deuteron in ^2H_2O) at C-2 completes the reaction and produces an enamine species (*FS*). Hydrolysis of this species (k_2) generates product **8**, whereas tautomerization (k'_4) results in the formation of the imine *FS′*. It is the reduction of this

dx.doi.org/10.1021/ja206873f | J. Am. Chem.Soc. 2012, 134, 293−304

species (*FS′*) with $NaBH_4$ (or $NaCNBH_3$) that inactivates *cis*-CaaD.[37] In the absence of $NaCNBH_3$, **8** could be generated by the other two routes shown in Scheme 7, or by a combination of these routes. In the first route, the imine (i.e., *FS′*) undergoes hydrolysis (k'_5) to produce **8**. In the second route, the imine tautomerizes (k_6) to the thermodynamically more stable enamine *FS″*, followed by hydrolysis through an addition elimination-type reaction initiated by the attack of water at C-3 (of the adduct).

The proposed scenarios in Scheme 7 are supported by trapping experiments and the global fit of the pre-steady state and steady state kinetic data (including the SVD analysis of time-resolved spectra). The minimal kinetic model required to completely account for all of the experimental data (Figure 4) is shown in Scheme 6 (see Text S3 in SI). Trapping experiments coupled with MS analysis (Figure 2 and Figure S3 of SI) and inhibition studies (Figure 3) are consistent with the formation of an adduct between Pro-1 and **7**. The electrophilic C3 carbon of **7** is the most favorable site (Scheme 7, *ES*) for an irreversible nucleophilic attack by the prolyl nitrogen. The stereochemistry of the reaction product (**8**) indicates that a proton is stereoselectively incorporated at C2 (Scheme 7, gray proton). Thus, the *FS* species in our model corresponds to the enamine shown in Scheme 7. The hydration of this species is expected to be the predominant route of breakdown (k_2), which is also consistent with the relatively high value of k_2 determined by simulation (Table 2).

The second possible route for the transformation of the *FS* species (k'_4) involves the formation of the reactive imine species (Scheme 7, *FS′*) by tautomerization. The resulting species, *FS′*, an iminium cation, is readily hydrolyzed.[38] Therefore, a hydrolysis step (k'_5) rather than a reversible formation step (Scheme S2 in SI, k'_{-4}) is more likely, although the latter possibility cannot be ruled out. The transient nature of the *FS′* species (Figure S9 of SI) is also consistent with the transient kinetic phase in the stopped-flow data attributed to it (i.e., Figure S7 of SI) and the associated difficulties in accurately defining the values of k'_4 and k'_5. As shown in the upper inset of Figure S9 of SI, the concentration of the *FS′* species is only predicted to exceed that of *FS″* (dominant fluorescent species) during the first 0.8 s of reaction. Moreover, the global fit predicts that the lifetimes of both the *FS′* and *FS* species are very similar (Figure S9 of SI).

The imine species (*FS′*) could also tautomerize (k_6) to a more thermodynamically stable enamine form (Scheme 7, *FS″*). This species, stabilized by conjugation of the double bond with the carboxylate group, would be the least susceptible to hydrolysis, consistent with the relatively slow breakdown of the intermediate (k_7 = 0.052 s^{-1}) predicted by SVD analysis and the global fit. Moreover, the spectral characteristics of this intermediate (λ_{max} 285 nm; $\varepsilon \approx 4500$ M^{-1} cm^{-1}) are similar to those of related enamines. For example, ethyl 3−amino-crotonate and ethyl *β*-cyanomethyl-aminocrotonate exhibit extinction coefficients of ∼16,000 M^{-1} cm^{-1} at a λ_{max} of 275 and 270 nm, respectively.[39,40] Also, enamines from malonate semialdehyde and penicillamine sulfinates typically absorb strongly in the region of 260−300 nm with large extinction coefficients (ε ∼10,000−30,000 M^{-1} cm^{-1}).[41,42] However, these model compounds are all based on reactions with primary amines and the extinction coefficients are measured in aqueous solution. In contrast, the *FS″* intermediate involves a reaction with a secondary amine (i.e., Pro-1)[43] which, when coupled with the electrostatic properties of the *cis*-CaaD active site environment, could account for the lower extinction coefficient observed.

The breakdown of the enamine *FS″* could alternatively correspond to the thermodynamically unfavorable reversible formation of the imine *FS′* (Scheme S2 [SI], k_{-6}).[44] However, in view of the extensive network of water molecules at the active site (Scheme 2),[10] hydrolysis of this enamine (presumably via an addition elimination-type reaction) is a more likely possibility. Thus, the reaction pathways shown in Scheme 7 are consistent with the minimal kinetic model required to account for all of the kinetic data (Scheme 6) and remain the preferred routes of the *cis*-CaaD catalyzed conversion of **7** to **8**.

The combined results implicate a covalent intermediate (i.e., *FS*) in the *cis*-CaaD-catalyzed transformation of **7** to **8**, and raise three questions. First, is this intermediate suggestive of a covalent intermediate in the *cis*-CaaD-catalyzed dehalogenation of **2** or is it a function of the reactivity of the allene? Second, is the body of knowledge for *cis*-CaaD, including the presumed pK_a of Pro-1 (∼9.3), consistent with a covalent intermediate in the enzymatic transformation of **7** and **2** (if an intermediate forms between **2** and enzyme)? Finally, are allene compounds appropriate probes for a stereochemical analysis of the *cis*-CaaD reaction using **2** because they may be processed by a different mechanism?

A large body of mechanistic and structural studies now exists for cofactor independent enzyme-catalyzed hydrolytic dehalogenation reactions.[45,46] Three groups of enzymes, the haloalkane dehalogenases, the haloacid dehalogenases, and 4-chlorobenzoyl-CoA dehalogenase, effect catalysis via a covalent ester intermediate,[47,48] whereas *cis*-CaaD and *trans*-3-chloroacrylic acid dehalogenase (CaaD) do not proceed through a covalent ester intermediate. In the first three groups, the carboxylate group of an active site aspartate attacks the halide-bearing carbon in an S_N2 type reaction to form a covalent ester intermediate and release the halide. Ester hydrolysis by an enzyme-activated water molecule releases enzyme and the alcohol product. In *cis*-CaaD and CaaD, catalysis is postulated to occur by direct attack of an activated water molecule on the substrate, as detailed in Scheme 2.

CaaD is a tautomerase superfamily member that dehalogenates *trans*-3-haloacrylates by an analogous, but seemingly more economical mechanism.[11] CaaD is a heterohexamer consisting of three *α*-subunits and three *β*-subunits that is highly specific for the *trans*-isomer. In CaaD, *α*Glu-52 is proposed to activate water for attack at C-3 of the *trans*-isomer. Two arginine residues, *α*Arg-8 and *α*Arg-11, interact with the C-1 carboxylate group (to bind and polarize the substrate), and *β*Pro-1 provides a proton at C-2 to complete the reaction.[11] CaaD lacks Tyr-103 and His-28, and has no known counterparts. Sequence analysis first argued against an ester covalent intermediate in the CaaD (and *cis*-CaaD) reactions because the key residues to generate and hydrolyze an ester intermediate are not present. Moreover, the sequences of CaaD and *cis*-CaaD align with tautomerase superfamily members, and not those of dehalogenases utilizing an ester intermediate.[1,2,6] This analysis, however, does not rule out an intermediate between *β*Pro-1 of CaaD and substrate (or Pro-1 of *cis*-CaaD and **2**).

Preliminary pre-steady state kinetic studies (stopped-flow fluorescence and rapid-quench flow) with wild-type and mutant *cis*-CaaD and **2** (data not shown) provide some evidence for a mechanism involving covalent catalysis. While global fitting using in-line kinetic models proved insufficient to account for

all of these data, the results (particularly the full time course data) are most accurately reproduced by mechanisms that included a branched pathway, which, by comparison to the present results with **7**, could be suggestive of covalent catalysis. Additional experiments with *cis*-CaaD and **2**, conducted at different pH values and with various mutants of *cis*-CaaD (data not shown), also suggest that the partitioning of the reaction (e.g., direct hydration vs covalent catalysis) changes as a function of these two variables, with some experimental results approximating those observed with **7**. Whether or not this branched pathway represents covalent catalysis is being investigated. It is also important to note that conventional fitting of the data to equations based upon simplified models would have been inadequate and would have failed to afford the fine distinction between branched and linear pathways. The rigorous standards set by globally fitting a large data set to a single, complete model allowed resolution of a branched pathway, which may be more common then currently believed.

Allenes are noted for their reactivity.[49] This feature has been exploited in the design of synthetic strategies and mechanism-based inhibitors.[49,50] In the latter, an acetylenic species is rearranged in an enzyme-catalyzed process to generate an allene, which can then alkylate an active site residue. The reactions of Δ^5-3-ketosteroid isomerase (KSI) with various acetylene steroidal compounds are well studied examples.[51,52] Several lines of evidence support the KSI-catalyzed rearrangement of the acetylene to an allene, and subsequent enzyme inactivation by the allene.[52] In the same way, **7** binds at the active site and "alkylates" Pro-1. However, the enzyme is not inactivated because the adduct is removed by an ensuing hydration reaction.

At first glance, two observations are inconsistent with the formation of a covalent intermediate between Pro-1 and **2** (or **7**). First, as noted above, the pK_a of Pro-1 (~9.3) suggests that the reaction of the amino-terminal proline with substrate could only occur with a small fraction of the enzyme at pH 8. The pK_a of βPro-1 in CaaD was measured by ^{15}N NMR spectroscopy (using uniformly ^{15}N-labeled CaaD), and found to be ~9.3.[13] This observation suggests that at biological pH, βPro-1 is largely cationic (and not nucleophilic). The pK_a of Pro-1 in *cis*-CaaD has not been measured by ^{15}N NMR spectroscopy, but it is presumed to be ~9.3, based on pH rate studies.[12] It can be reasonably argued that the reaction of the small fraction of enzyme bearing the nucleophilic Pro-1 with **2** (or **7**) perturbs the equilibrium so that more enzyme reacts. In this way, the reaction is driven to completion.[53] A second issue is the proposed role of Pro-1 in *cis*-CaaD: it functions as a general acid catalyst, and provides the proton that completes the conjugate addition of water to **2** (Scheme 2). However, the covalent attachment of Pro-1 to the allene could preclude such a role so that hydration occurs by a route not involving Pro-1. One possible route could involve Glu-114 and Tyr-103 and their interaction with the network of water molecules.[10]

Neither observation rules out covalent catalysis for the dehalogenation of **2**. The remaining mechanistic and structural evidence for the reaction of *cis*-CaaD and **2** could be consistent with a mechanism involving direct hydration or covalent catalysis.[6] To date, a covalent intermediate has not been detected between *cis*-CaaD and **2**, with only the results of this study and additional stopped-flow fluorescence experiments (above) suggesting the possibility. Although this work implicates covalent catalysis in the transformation of **7** to **8**, it remains unknown whether the *cis*-CaaD-catalyzed dehalogenation of **2** proceeds by covalent catalysis alone or whether some percentage of the reaction proceeds by covalent catalysis in conjunction with the direct hydration route postulated previously (Scheme 2).

Finally, these results have implications for the proposed stereochemical analysis of *cis*-CaaD using allene compounds. One intent of a stereochemical analysis is to indicate the position of the active site residues relative to the substrate: a *syn* addition of water places the reactive groups on the same side of the substrate, whereas an *anti* addition places them on opposite sides of the substrate.[54] Because allene compounds can be made chiral by substitution,[55] it was thought that the reaction of one enantiomer (in this case, substitution at C-4 of **7**) coupled with a stereochemical analysis of deuteron incorporation at C-2 would enable us to infer the overall stereochemical course of the reaction using **2**. It is unclear if this approach can be used to infer the stereochemical course of the reaction using **2**, but it can be used to determine the stereochemical course of the reaction using **7**. Such an analysis could shed light on the mechanism for hydration of the covalent intermediate.

5. CONCLUSION

Trapping experiments ($NaCNBH_3$), MS analysis, and inhibition assays indicate that the *cis*-CaaD catalyzed hydration of **7** proceeds exclusively by covalent formation of an enamine with the *N*-terminal active site residue, Pro-1. Global fitting of the entire pre-steady state and full progress kinetic data sets (including SVD analysis of time-resolved spectra) was successfully accomplished using a single, simple model which invoked a branched pathway, consistent with enamine−imine tautomerization of the covalent adduct and subsequent hydration. This represents the first reported observation of a tautomerase superfamily member functioning by covalent catalysis, which may also contribute to the catalytic action of this enzyme toward other substrates.

■ ASSOCIATED CONTENT

Supporting Information

Equations for the fitting of irreversible inhibition data and the absorbance of fluorescence excitation radiation, additional ^{1}H NMR spectra, ESI-MS and MALDI-MS results, additional analysis of stopped-flow data, kinetic schemes and fitting results used to evaluate the final global model, and an analysis of the FitSpace confidence contours. This material is available free of charge via the Internet at http://pubs.acs.org.

■ AUTHOR INFORMATION

Corresponding Author

whitman@mail.utexas.edu

Notes

Kenneth A. Johnson is President of KinTek Corp.

■ ACKNOWLEDGMENTS

Positive mode ESI and MALDI mass spectrometry were performed by the ICMB Protein and Metabolite Analysis Facility (University of Texas at Austin). We thank Dr. Karen Allen (Boston University) for the AAD expression plasmid. Stopped-flow instruments and KinTek Explorer data analysis software were provided by KinTek Corp. This research was supported by the National Institutes of Health Grant GM-65324 (C.P.W.), the Robert A. Welch Foundation Grant F-

1334 (C.P.W.), and a fellowship award (F32 GM089083) from the National Institute of General Medical Sciences to G.K.S.

REFERENCES

(1) Poelarends, G. J.; Serrano, H.; Person, M. D.; Johnson, W. H. Jr.; Murzin, A. G.; Whitman, C. P. *Biochemistry* **2004**, *43*, 759.

(2) Poelarends, G. J.; Saunier, R.; Janssen, D. B. *J. Bacteriol.* **2001**, *183*, 4269.

(3) Poelarends, G. J.; Wilkens, M.; Larkin, M. J.; Van Elsas, J. D.; Janssen, D. B. *Appl. Environ. Microbiol.* **1998**, *64*, 2931.

(4) Van Hylckama Vlieg, J. E. T.; Janssen, D. B. *Biodegradation* **1992**, *2*, 139.

(5) Hartmans, S.; Jansen, M. W.; Van der Werf, M. J.; De Bont, J. A. M. *J. Gen. Microbiol.* **1991**, *137*, 2025.

(6) Poelarends, G. J.; Veetil, V. P.; Whitman, C. P. *Cell. Mol. Life Sci.* **2008**, *65*, 3606.

(7) Murzin, A. G. *Curr. Opin. Struct. Biol.* **1996**, *6*, 386.

(8) Poelarends, G. J.; Serrano, H.; Person, M. D.; Johnson, W. H.; Whitman, C. P. *Biochemistry* **2008**, *47*, 8139.

(9) Poelarends, G. J.; Whitman, C. P. *Bioorg. Chem.* **2004**, *32*, 376.

(10) De Jong, R. M.; Bazzacco, P.; Poelarends, G. J.; Johnson, W. H. Jr.; Kim, Y. J.; Burks, E. A.; Serrano, H.; Thunnissen, A.-M. W. H.; Whitman, C. P.; Dijkstra, B. W. *J. Biol. Chem.* **2007**, *282*, 2440.

(11) De Jong, R. M.; Brugman, W.; Poelarends, G. J.; Whitman, C. P.; Dijkstra, B. W. *J. Biol. Chem.* **2004**, *279*, 11546.

(12) Poelarends, G. J.; Serrano, H.; Johnson, W. H. Jr.; Whitman, C. P. *Biochemistry* **2004**, *43*, 7187.

(13) Azurmendi, H. F.; Wang, S. C.; Massiah, M. A.; Poelarends, G. J.; Whitman, C. P.; Mildvan, A. S. *Biochemistry* **2004**, *43*, 4082.

(14) Robertson, B. A.; Schroeder, G. K.; Jin, Z.; Johnson, K. A.; Whitman, C. P. *Biochemistry* **2009**, *48*, 11737.

(15) Wang, S. C.; Person, M. D.; Johnson, W. H. Jr.; Whitman, C. P. *Biochemistry* **2003**, *42*, 8762.

(16) Eglinton, G.; Jones, E. R. H.; Mansfield, G. H.; Whiting, M. C. *J. Chem. Soc.* **1954**, 3197.

(17) Lian, H.; Whitman, C. P. *J. Am. Chem. Soc.* **1993**, *115*, 7978.

(18) Stanley, T. M.; Johnson, W. H. Jr.; Burks, E. A.; Whitman, C. P.; Hwang, C.-C.; Cook, P. F. *Biochemistry* **2000**, *39*, 718.

(19) Ho, M.-C.; Menetret, J.-F.; Tsuruta, H.; Allen, K. N. *Nature* **2009**, *459*, 393.

(20) Waddell, W. J. *J. Lab. Clin. Med.* **1956**, *48*, 311.

(21) Bradford, M. M. *Anal. Biochem.* **1976**, *72*, 248.

(22) Houmard, J.; Drapeau, G. R. *Proc. Natl. Acad. Sci. U.S.A.* **1972**, *69*, 3506.

(23) Bruice, P. Y. *J. Am. Chem. Soc.* **1990**, *112*, 7361.

(24) Johnson, K. A.; Simpson, Z. B.; Blom, T. *Anal. Biochem.* **2009**, *387*, 20.

(25) Johnson, K. A.; Simpson, Z. B.; Blom, T. *Anal. Biochem.* **2009**, *387*, 30.

(26) The commercially available **8** (δ 2.076 3H, s, C4) also contained an unknown impurity (δ 2.05).

(27) Pro-1, the only active site residue of the Pro-1-Asp-26 peptide, was previously shown to be the only site modified by various irreversible covalent inhibitors.[10,12]

(28) Control experiments monitoring the enzyme alone were also conducted, and adjustments were made to the data to correct for slight background changes in enzyme absorbance as a function of time.

(29) For instance, the amplitude eigenvector dominated by the intermediate *FS″* (teal/green) exhibits both a formation and decay phase, and the fitted scaling factor corresponding to the individual species *FS″* is the most significant. Also, the amplitude eigenvectors are not scaled according to their singular value (eigenvector magnitude), and some of them are negative, reflecting the fact that only the product of the spectra and amplitude eigenvectors are constrained to be positive.

(30) In both cases, the reconstructed data sets begin at time zero, whereas the first experimental traces begin at 1.4 s.

(31) Johnson, K. A. Transient-state kinetic analysis of enzyme reaction pathways. In *The Enzymes*, 3rd ed.; Sigman, D. S., Ed.; Academic Press: San Diego, 1992; Vol. *20*.

(32) The 'irreversible' formation and decay of *FS″* (Scheme 5) could conceivably represent 'net' rate constants, or in a kinetically equivalent model, the off-pathway step could represent the equilibrium formation of *FS″* as a 'dead-end' complex (Scheme S1, SI).

(33) As observed with the previous model, the kinetic data can be fit to the alternative model shown in Scheme S2 (SI), in which the formation and decomposition of the *FS″* complex represents an equilibrium step (K_6), with $k_{-6} \approx k_7$ (see Discussion).

(34) Chance, B. *J. Biol. Chem.* **1943**, *151*, 553.

(35) Singh, S.; Ballou, D. P.; Banerjee, R. *Biochemistry* **2011**, *50*, 419.

(36) Enzymatic catalysis via Schiff base formation involving an *N*-terminal proline residue has literature precedents in the mechanism of formamidopyrimidine-DNA glycosylase: Zharkov, D. O.; Rieger, R. A.; Iden, C. R.; Grollman, A. P. *J. Biol. Chem.* **1997**, *272*, 5335.

(37) $NaCNBH_3$ reduction of **7** with *cis*-CaaD afforded nearly complete labeling of the protein with the decarboxylated mass of **7**. One possible explanation is that accommodation of both compounds at the active site could introduce steric strain (e.g., bending) in the imine [of **7**], facilitating its subsequent decarboxylation.[19]

(38) Eldin, S.; Jencks, W. P. *J. Am. Chem. Soc.* **1995**, *117*, 4851.

(39) Dixon, K.; Greenhill, J. V. *J. Chem. Soc., Perkin Trans. 2* **1974**, 164.

(40) Guthrie, J. P.; Jordan, F. *J. Am. Chem. Soc.* **1972**, *94*, 9132.

(41) Brenner, D. G.; Knowles, J. R.; Rihs, G. *Biochemistry* **1981**, *20*, 3680.

(42) Kemal, C.; Knowles, J. R. *Biochemistry* **1981**, *20*, 3688.

(43) The nitrogen of a pyrrolidine enamine can also exhibit significant sp^2 character: Pihko, P. M.; Majander, I.; Erkkila, A. *Top. Curr. Chem.* **2010**, *291*, 29.

(44) Guthrie, J. P.; Jordan, F. *J. Am. Chem. Soc.* **1972**, *94*, 9136.

(45) Copley, S. D. Microbial dehalogenases. In *Comprehensive Natural Products Chemistry*; Poulter, C. D., Ed.; Elsevier Science Ltd.: Oxford, 1999; Vol. *5*, pp 401–422.

(46) Janssen, D. B. *Curr. Opin. Chem. Biol.* **2004**, *8*, 150.

(47) Benning, M. M.; Taylor, K. L.; Liu, R.-Q.; Yang, G.; Xiang, H.; Wesenberg, G.; Dunaway-Mariano, D.; Holden, H. M. *Biochemistry* **1996**, *35*, 8103.

(48) Verschueren, K. H. G.; Seljee, F.; Rozeboom, H. J.; Kalk, K. H.; Dijkstra, B. W. *Nature (London)* **1993**, *363*, 693.

(49) Ma, S. *Acc. Chem. Res.* **2009**, *42*, 1679.

(50) Hoffmann-Roeder, A.; Krause, N. *Angew. Chem., Int. Ed.* **2004**, *43*, 1196.

(51) Covey, D. F.; Robinson, C. H. *J. Am. Chem. Soc.* **1976**, *98*, 5038.

(52) Schwab, J. M.; Henderson, B. S. *Chem. Rev.* **1990**, *90*, 1203.

(53) Given the unique reactivity of **7**, the possibility exists that the reaction could alternatively proceed via electrophilic addition, with proton donation by Pro-1. For example: Cramer, P.; Tidwell, T. *J. Org. Chem.* **1981**, *46*, 2683.

(54) Sakai, A.; Fedorov, A. A.; Fedorov, E. V.; Schnoes, A. M.; Glasner, M. E.; Brown, S.; Rutter, M. E.; Bain, K.; Chang, S.; Gheyi, T.; Sauder, J. M.; Burley, S. K.; Babbitt, P. C.; Almo, S. C.; Gerlt, J. A. *Biochemistry* **2009**, *48*, 1445.

(55) Schwab, J. M.; Lin, D. C. T. *J. Am. Chem. Soc.* **1985**, *107*, 6046.